Supplementary Information

Electrocatalytic Nitrate Reduction over Cu_2O Nanowires Partially Decorated with Fe_2O_3 Nanoparticles

Kaili Liu,†[a] Zhehao Sun,†[a] Muhammad Usman,[a] Jiayi Chen,[a] Myat Naing,[a] Huiming Gu,[a] Yi-lun Chen,[a] Yiding Yang,[a] Hang Yin,[a] Ary Anggara Wibowo,[b] Xuechen Jing,[a] Nicholas Cox[a] and Zongyou Yin*[a]

1.1 Experimental method

The fabrication of $Cu(OH)_2$ nanowires on Cu foam: In general, $1 \times 3\ cm^2$ Cu foam was first washed with the mixture of acetone, ethanol and water, subsequently soak the Cu foam in 0.1 M HCl to clean the surface oxide and put it in the vacuum oven under 60℃ for 6h to dry it . Then the cleaned Cu foil was soaked in the solution which contains 0.1 M $(NH_4)_2S_2O_8$ and 1 M NaOH for 30 minutes to form $Cu(OH)_2$ nanowires on Cu foil ($Cu(OH)_2$ NW).

The fabrication of xFe_2O_3/Cu_2O: The as-prepared $Cu(OH)_2$ NF was immersed in 1mM $FeCl_2$ solution for 1h and washed with water, and then put it in the oven under 60℃ for 6h to dry it. Finally, the as-prepared sample was reduced under -0.4V vs. RHE for 1h to obtain $0.01Fe_2O_3/Cu_2O$. The content of Fe_2O_3 can be tuned by changing the concentrations of $FeCl_2$ solution to 0.05M, 2mM and 3mM for fabricate $0.067Fe_2O_3/Cu_2O$ $0.2Fe_2O_3/Cu_2O$ $0.3Fe_2O_3/Cu_2O$, respectively. While the pure Cu_2O sample was synthesized by reducing the $Cu(OH)_2$ nanowires on Cu foam under -0.4V vs. RHE for 1h.

1.2 Materials characterization

X-ray diffraction (XRD, Bruker Xray diffractometer) using a Cu Kα radiation source was employed to determine the phase composition of the catalysts. The morphology,

composition, and elemental distribution of the catalysts were characterized using scanning electron microscopy (SEM, Zeiss UltraPlus Field emission scanning electron microscope) and transmission electron microscopy (TEM, JEOL 2100F FEGTEM). The surface elemental composition and oxidation states were analyzed by X-ray photoelectron spectroscopy (XPS, Kratos AXIS Supra photoelectron spectrometer using monochromated Al Ka radiation, power 300W, Pass energy 20 eV for wide spectra and 5 eV for high resolution), with C 1s used as a reference for calibration. The metal content in the catalysts was quantified using inductively coupled plasma optical emission spectroscopy (ICP-OES). Ultraviolet-visible (UV-Vis) absorption spectra of the products were recorded using a UV-Vis spectrophotometer (UV-2700). Proton nuclear magnetic resonance (^{1}H NMR) analysis was performed on a Bruker Avance III 400 MHz NMR spectrometer.

1.3 Electrochemical measurements

The electrochemical nitrate reduction reaction (NO_3RR) was performed using a three-electrode system in an H-cell. xFe_2O_3/Cu_2O samples were used as the working electrode. Ag/AgCl and Pt foil were used as the reference and counter electrodes, respectively. Nafion-117 membranes were used to separate the two chambers of the H-cell. During the electrocatalysis tests, each chamber was filled with 40 mL of electrolyte (0.1 M K_2SO_4 with 1000 ppm KNO_3). Potentiostatic tests were conducted during NO_3RR at different potentials under ambient conditions after 30 min of purging with Ar (99.999%). After 30 min of electroreduction, the concentration of NH_3 in the electrolyte was measured using the Indophenol-blue method.

1.4 Estimation of ammonia

The liquid products generated from the electroreduction of NO_3^- were qualitatively and quantitatively analyzed using UV-Vis spectrophotometry.

Preparation of Colouring reagents:

Chromogenic reagent (A): 1.0 M NaOH solution containing 5 wt% sodium salicylate and 5 wt% potassium sodium tartrate.

Oxidizing solution (B): 0.05 M sodium hypochlorite (available chlorine 10-15 %) solution.

Catalysing reagent (C): 1 wt% sodium nitroferricyanide solution.

Preparation of NH_4^+ Standard Calibration Curve:

A volume of 2 mL from the standard solutions was transferred into test tubes, followed by the sequential addition of 2 mL of chromogenic reagent (A), 1 mL of oxidizing agent solution (B), and 0.2 mL of catalysing reagent (C). The mixtures were thoroughly shaken and allowed to stand for 1 hour. The concentration of the resulting indophenol blue was then determined using a UV-Vis spectrophotometer, with a scanning wavelength range of 550–750 nm. The standard curve was constructed by plotting absorbance at 655 nm (Y-axis) against the NH_3 concentration (X-axis)[1].

Fig. S8a displays that a set of standard ammonia solutions and their UV-vis absorbance curves were prepared to estimate the amount of ammonia in the samples. The prepared calibration curve exhibited an R-square value of 0.99906 (Fig. S8b), which shows that the model fits the data with good accuracy. To minimize possible interference from Fe^{3+}, Cu^{2+}, or OH^- ions in the colorimetric determination of NH_4^+, all measurements were conducted in neutral electrolyte (0.1 M K_2SO_4 + 0.01 M KNO_3) without any organic additives. The indophenol-blue method was cross-validated by isotope-labelling and ^1H NMR controls, confirming negligible background signal and ensuring the reliability of the colorimetric quantification in this system.

1.5 Nitrite quantification

Nitrite in the electrolyte was quantified by the Griess colorimetric assay. The chromogenic reagent was freshly prepared by dissolving 0.2 g N-(1-naphthyl)ethylenediamine dihydrochloride, 4.0 g sulfanilamide, and 10 mL H_3PO_4 in deionized (DI) water and diluting to 50 mL. For each measurement, 1 mL of post-electrolysis electrolyte was diluted with DI water to 5 mL, after which 0.1 mL of reagent was added. The mixture was thoroughly mixed and allowed to react for 20 min at ambient temperature. Absorbance was recorded at 540 nm on a UV–Vis spectrophotometer with scan range 400–700 nm. Calibration curves were constructed with standard NO_2^- solutions of defined concentrations. Fig. 9a shows UV–Vis spectra of standard nitrite solutions prepared to quantify nitrite in the samples. The corresponding calibration curve (Fig. 9b) exhibits excellent linearity (R^2 = 0.9992), confirming reliable concentration determination.

1.6 Calculations of the liquid products yield rate and Faradaic efficiency

The NH_3 yield rate was calculated using the following Reaction:

$$Y = (17 \times C \times V) / t \times A$$

The Faradaic efficiency was calculated using the following Reaction:

$$FE (\%) = (n \times F \times C \times V) / Q \times 100$$

where C is the measured liquid products concentration after nitrate reduction in the electrolyte, V is the volume of the electrolyte in the cathode compartment, t is electroreduction time, A is the geometric area of the working electrode, n is the number of electrons required to form the liquid products, F is the Faraday constant (96,485C/mol), and Q is the total charge transfer during electroreduction process[2].

1.7 ^{15}N Isotope Labelling Experiments

For the isotope labelling experiments, $K^{15}NO_3$ (98.3% enrichment, Sigma Aldrich) was utilized as the nitrogen source to trace the origin of ammonia. Electroreduction of nitrate to ammonia was performed at -0.4 V (vs. RHE) for 0.5 h in 0.1 M K_2SO_4 solution containing 1000 ppm $^{15}NO_3^-$. After the reaction, 0.6 mL of the liquid product was collected from the cathodic compartment and acidified with 0.1 mL of 3 M H_2SO_4. Subsequently, 700 µL of the acidified mixture was transferred into an NMR tube for ^{1}H NMR analysis. One-dimensional ^{1}H NMR spectra were recorded using a Bruker Avance-400 superconducting Fourier transform NMR spectrometer, with water peaks suppressed via the water pre-saturation method.

1.8 DFT calculation

Density Functional Theory (DFT) calculations were carried out using the Vienna Ab initio Simulation Package (VASP).[3, 4] The interaction between core and valence electrons was described using the Projector Augmented Wave (PAW) method,[5] and the exchange–correlation effects were treated with the Perdew–Burke–Ernzerhof (PBE) functional under the generalized gradient approximation (GGA) framework.[6] A plane-wave kinetic energy cutoff of 400 eV was applied throughout the calculations. The structural optimizations were performed until the total energy and atomic forces converged to within 10^{-4} eV and 10^{-2} eV/Å, respectively. To account for dispersion forces, Grimme's DFT-D3 correction was employed. [7] The Brillouin zone was sampled using a 3 × 3 × 1 Monkhorst-Pack k-point mesh. Electronic structure analyses were conducted using the VASPKIT post-processing toolkit. [8] For surface modeling, supercells comprising 80 atoms for Fe2O3 and 96 atoms for Cu2O were constructed, ensuring sufficient spatial separation to minimize periodic image interactions

during Gibbs free energy computations. A vacuum layer of at least 8 Å was added perpendicular to the slab surface to avoid artificial interlayer coupling.

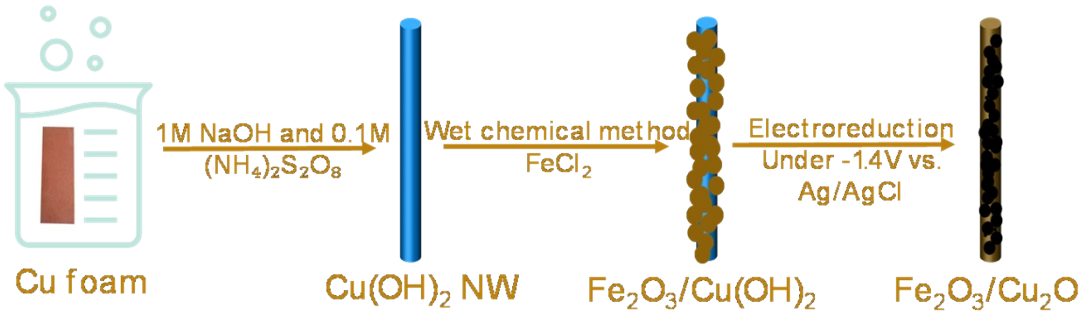

Fig. S1 The schematic process for fabricating Fe_2O_3/Cu_2O.

Table S1. ICP results of Fe and Cu among all samples.

Precursor	Cu(%)	Fe(%)	Name as
0.5mM $FeCl_2$	93.3	6.67	0.067 Fe_2O_3/Cu_2O
1mM $FeCl_2$	89.4	10.6	0.1 Fe_2O_3/Cu_2O
2mM $FeCl_2$	78.5	21.5	0.2 Fe_2O_3/Cu_2O
3mM $FeCl_2$	66.7	33.3	0.3 Fe_2O_3/Cu_2O

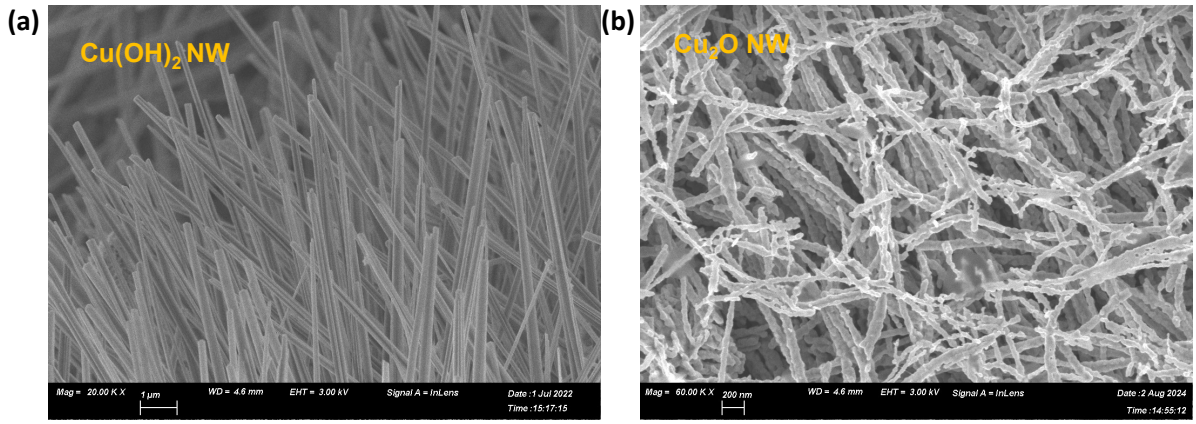

Fig. S2 The SEM images of $Cu(OH)_2$ NW (a) and Cu_2O NW (b).

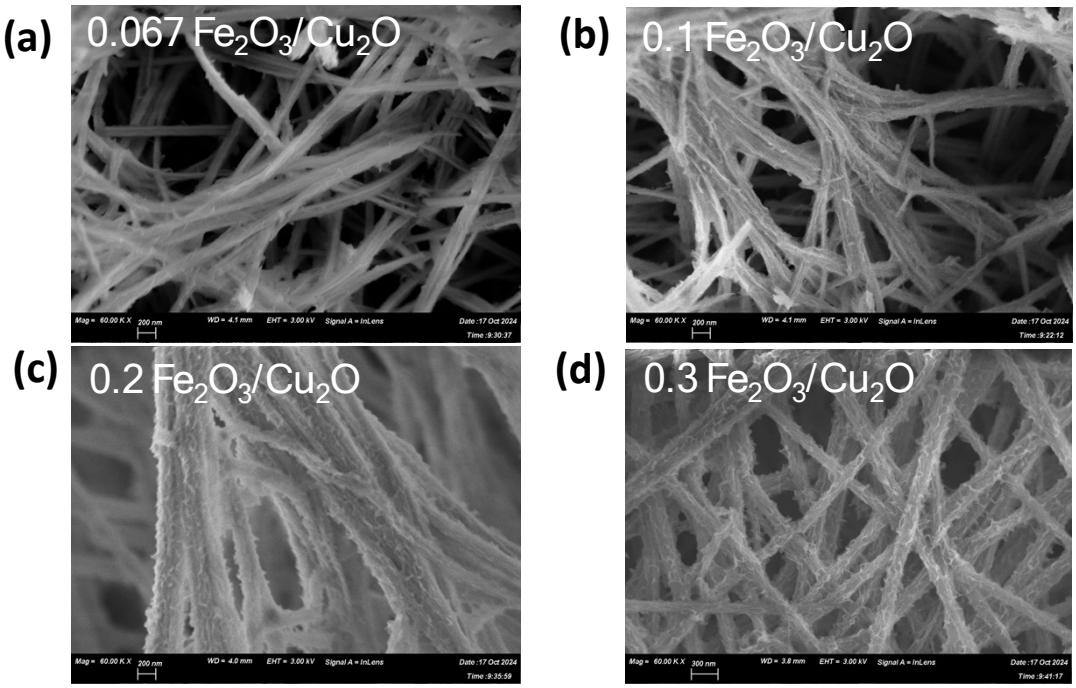

Fig. S3 SEM images of the pre-prepared 0.067 Fe_2O_3/Cu_2O (a), 0.1 Fe_2O_3/Cu_2O (b), 0.2 Fe_2O_3/Cu_2O (c) and 0.3 Fe_2O_3/Cu_2O (d).

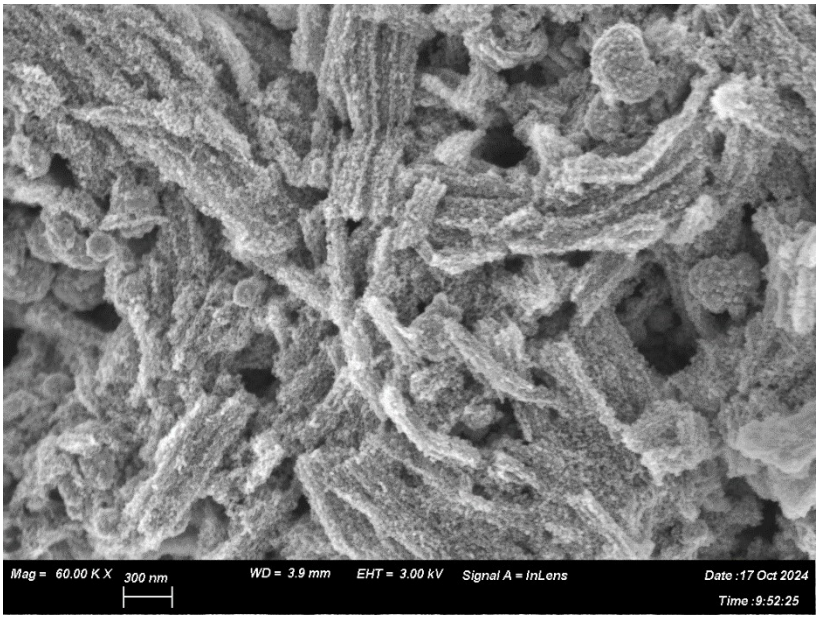

Fig. S4 SEM image of 0.1 Fe_2O_3/Cu_2O after 1h electroreduction under -0.4V Vs. RHE.

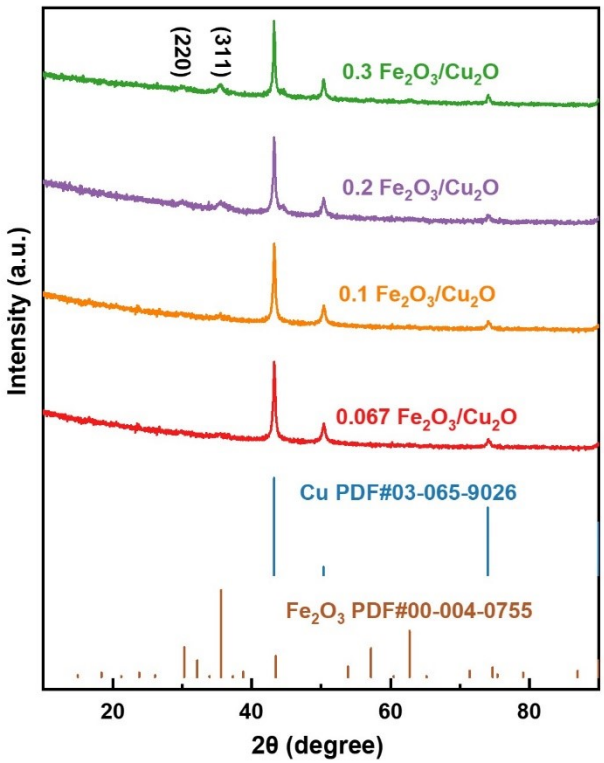

Fig. S5 XRD patterns of 0.067 Fe_2O_3/Cu_2O (a), 0.1 Fe_2O_3/Cu_2O (b), 0.2 Fe_2O_3/Cu_2O (c) and 0.3 Fe_2O_3/Cu_2O (d).

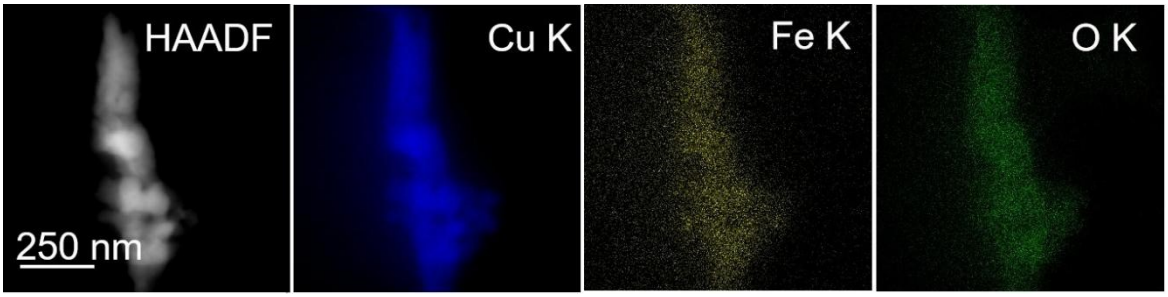

Fig. S6 EDS mapping of 1mM $FeCuO_x$.

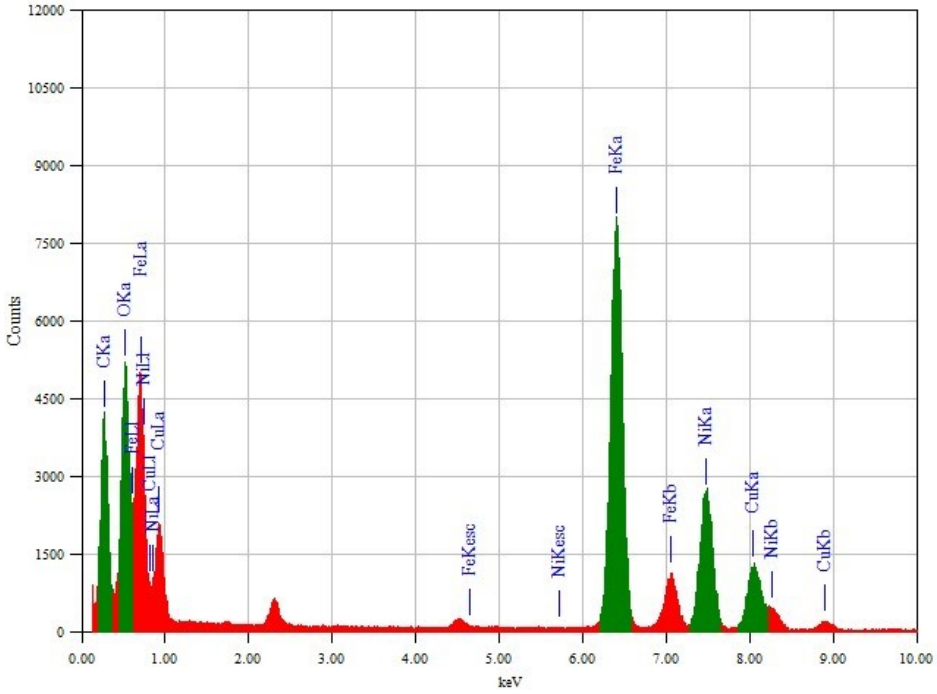

Fig. S7 EDS spectra of 1mM $FeCuO_x$.

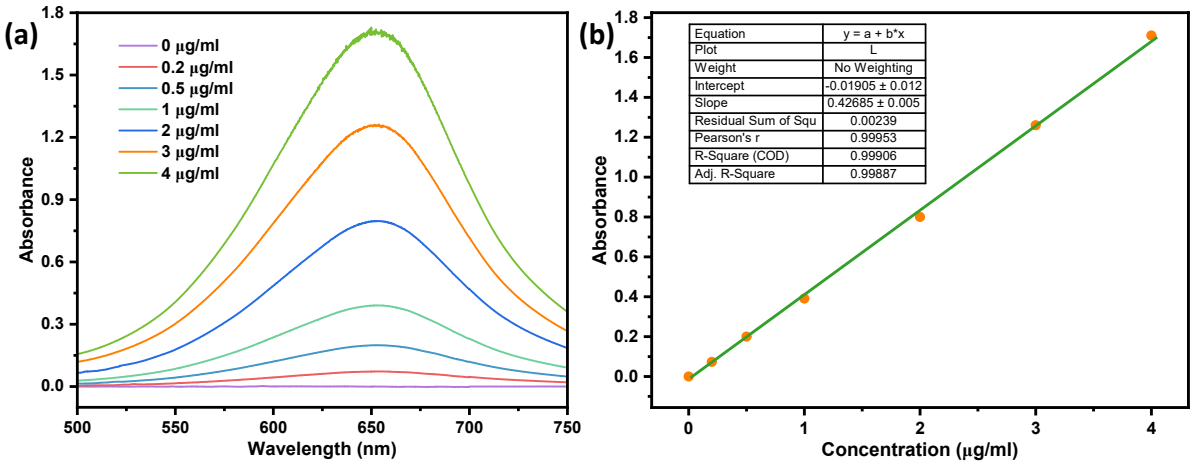

Fig. S8 (a) UV-Vis absorption spectra of NH_4Cl assays after incubation for 1h at ambient conditions and its Calibration curve used for the calculation of NH_3 concentrations (b).

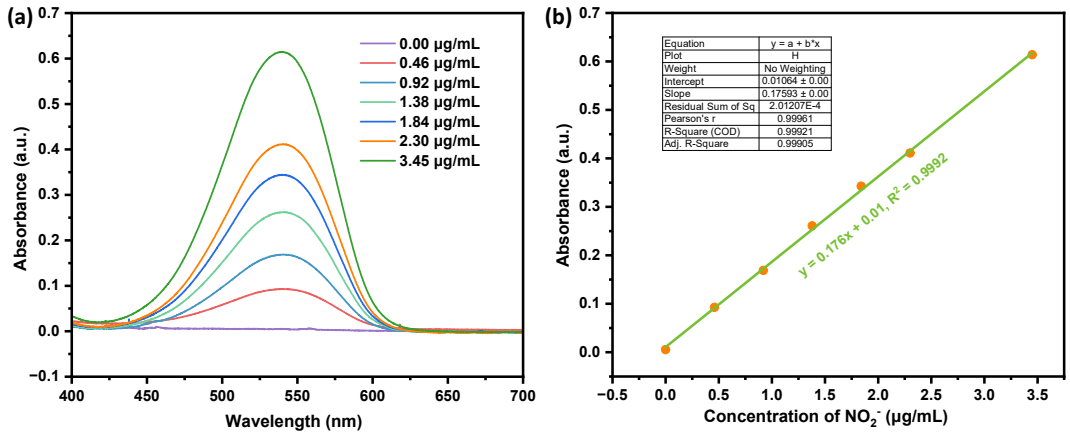

Fig. S9 UV–Vis absorption spectra of nitrite (a) and the corresponding calibration curve for quantifying nitrite concentration (b).

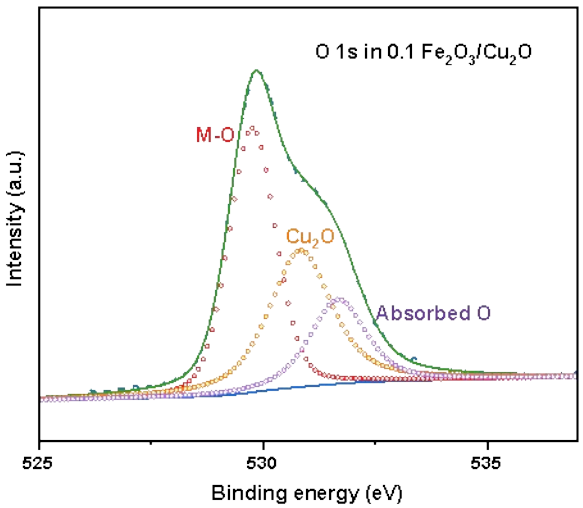

Fig. S10 XPS spectra of O 1s in 0.1 Fe_2O_3/Cu_2O.

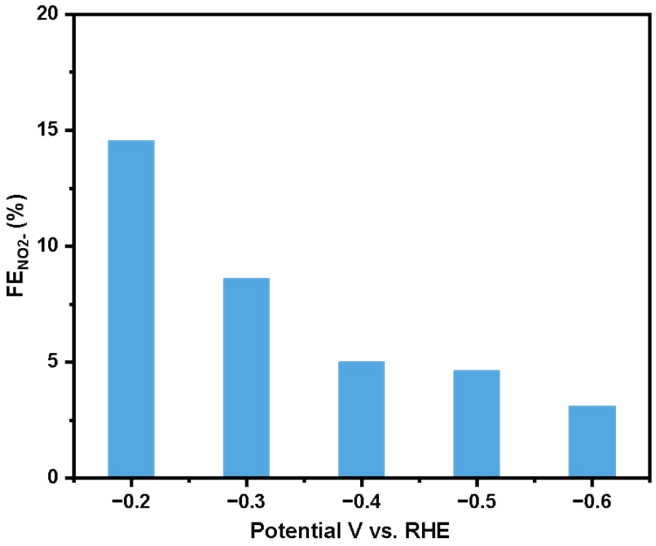

Fig. S11 The NO_2^- FE of $0.1Fe_2O_3/Cu_2O$ under various potentials.

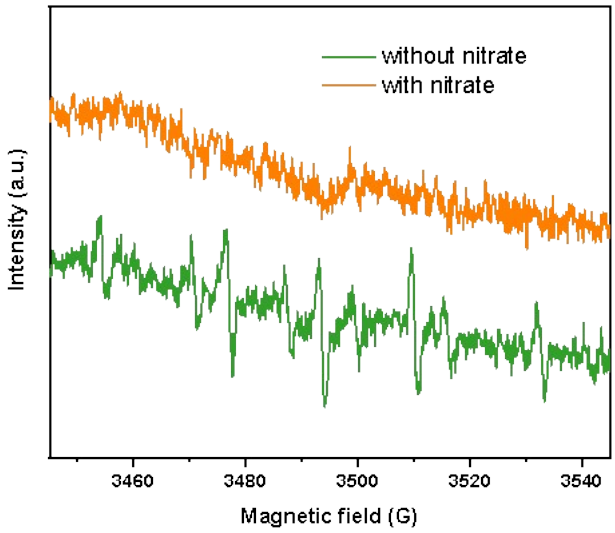

Fig. S12 EPR spectra of 0.1 Fe_2O_3/Cu_2O reacted in the electrolytes with and without nitrate.

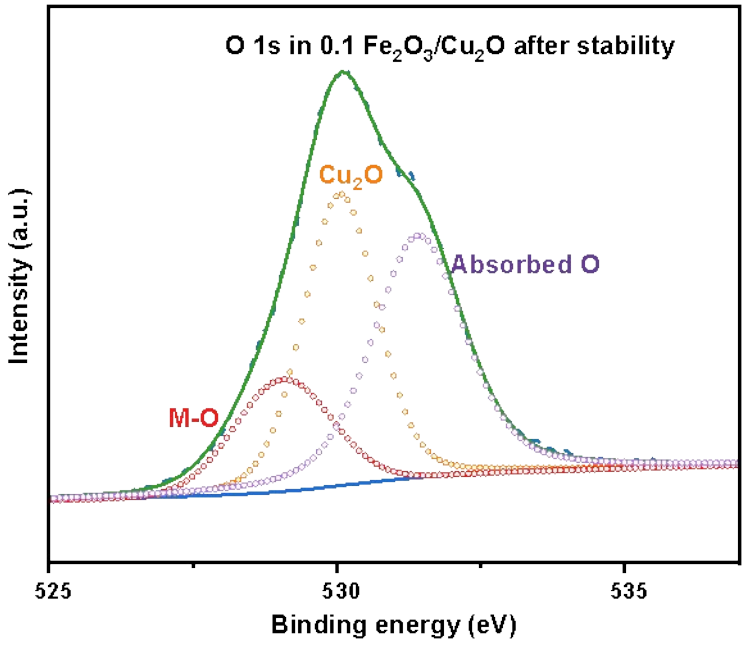

Fig. S13 XPS spectra of O 1s in 0.1 Fe_2O_3/Cu_2O after stability test. Compared with Fig. S10, a moderate variation in the relative intensities of the M-O and adsorbed oxygen components is observed, which may reflect slight surface reorganization or increased hydroxylation during prolonged operation, while the overall lattice oxygen framework remains largely preserved.

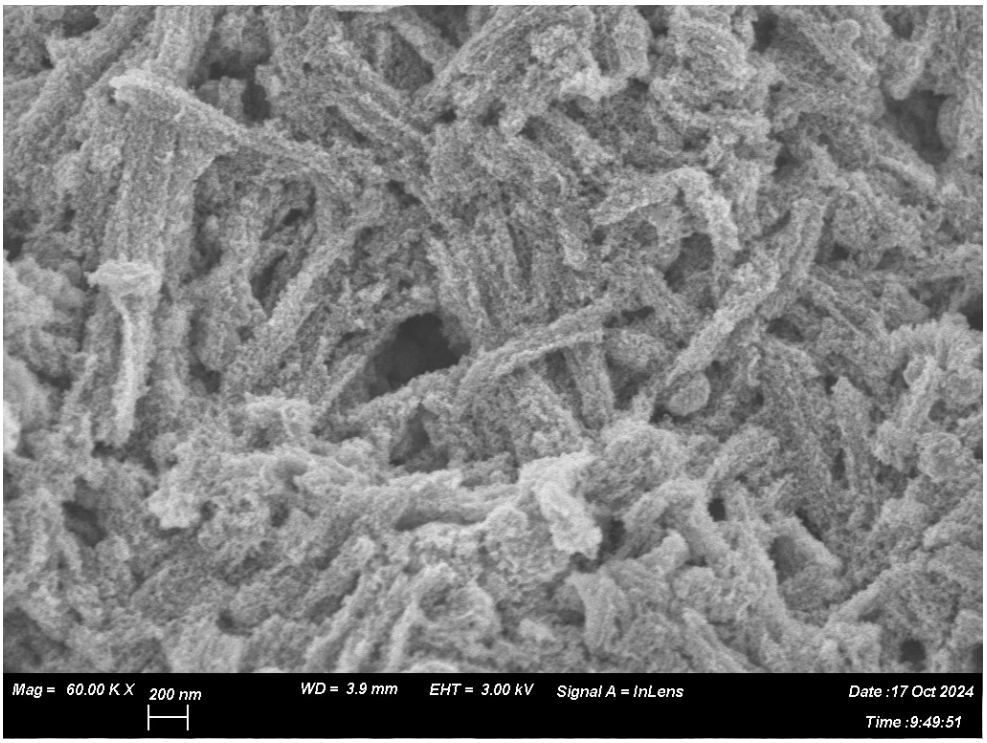

Fig. S14 SEM image of 0.1 Fe_2O_3/Cu_2O after stability test.

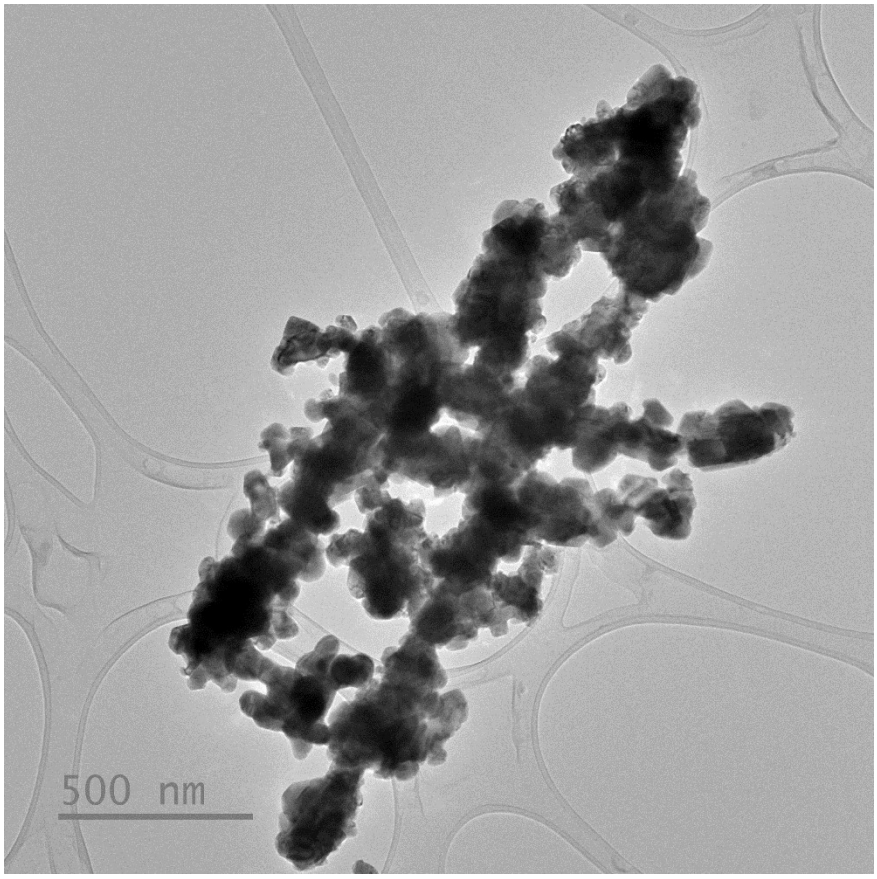

Fig. S15 TEM image of 0.1 Fe_2O_3/Cu_2O after stability test.

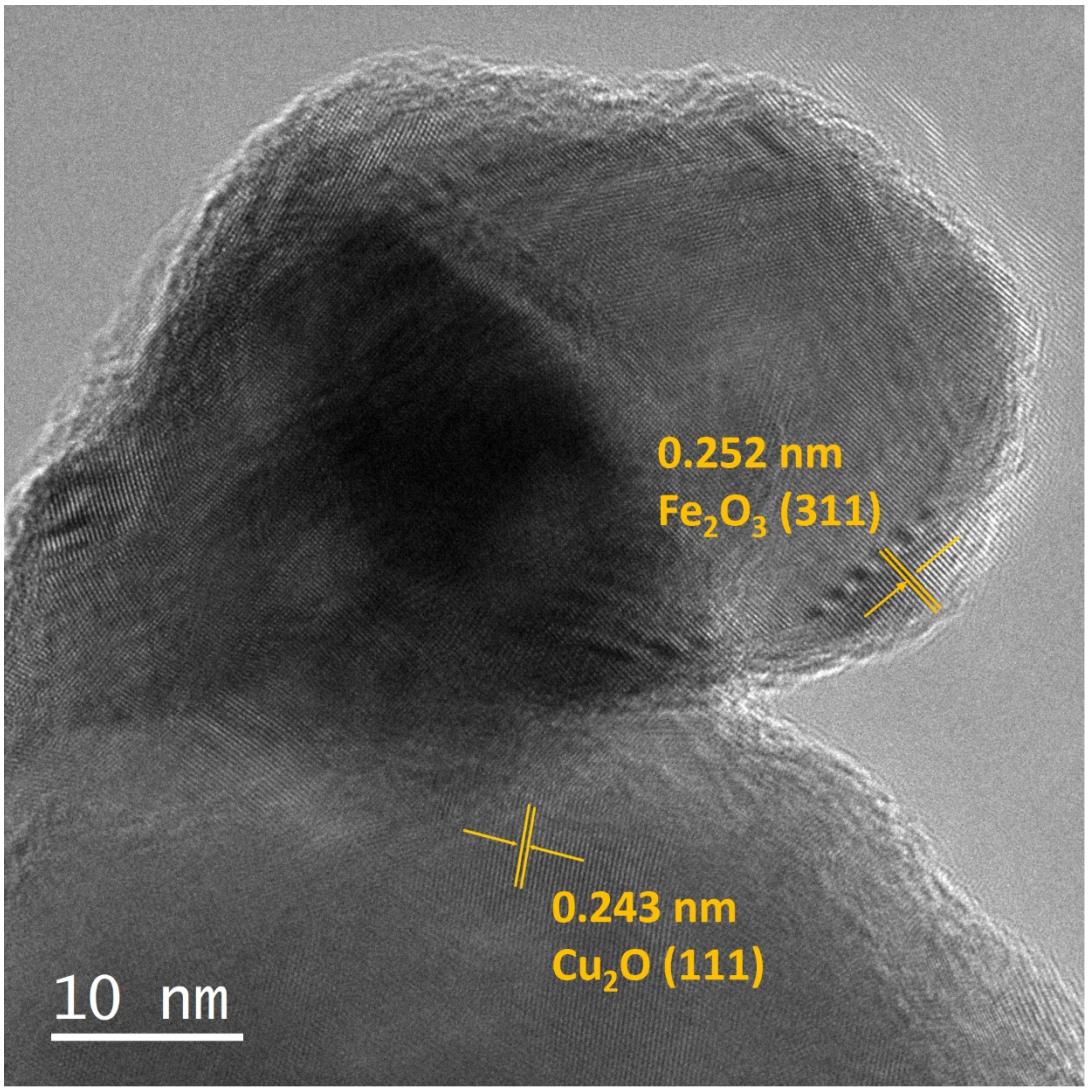

Fig. S16 HRTEM result of 0.1 Fe_2O_3/Cu_2O after stability test.

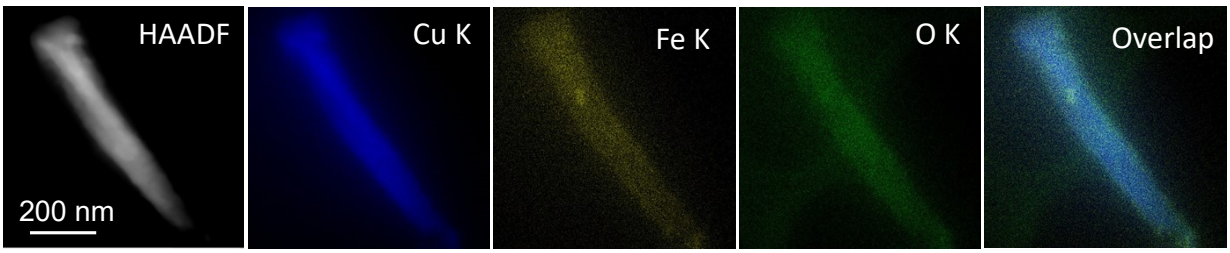

Fig. S17 TEM mapping images of 0.1 Fe_2O_3/Cu_2O after stability test.

Table S2. The NH_3 performance comparison among various iron-based catalysts.

Catalyst	NH_3 yield	Faradaic efficiency	Potential (vs RHE)	Electrolyte	Stability cycles	Reference
Fe-Co_3O_4 Nanoarray/Ti Mesh	0.624 mg mg cat^{-1} h^{-1}	95.5	− 0.7	0.1 M PBS + 50 mM NO_3^-	5 cycles, 9 h	[9]
Fe/Ni_2P	4.17 mg h^{-1} cm^{-2}	94.3	− 0.4	0.2 M K_2SO_4 + 50 mM KNO_3	6 cycles, 11 h	[10]
Fe_2TiO_5	0.73 mmol mg cat^{-1} h^{-1}	87.6	− 1.0	PBS + 0.1 M $NaNO_3$	12 cycles, 24 h	[11]
$LaxFeO_{3-\delta}$	1024.8 μg h^{-1} cm^{-2} @− 1.0 V vs. RHE	78.1	− 0.8	0.1 M Na_2SO_4 + 0.1 M $NaNO_3$	4 cycles	[12]
Cu/Fe-TiO_2	NA	91.2	− 1.4 V vs. SCE	0.5 M Na_2SO_4 + 50 ppm NO_3^-	5 cycles, 16 h	[13]
Fe_3O_4 @TiO_2/TP	12394.3 μg h^{-1} cm^{-2}	88.4	− 0.9	0.1 M PBS + 0.1 M $NaNO_3$	12 cycles, 12 h	[14]

References

1. L. Li, C. Tang, B. Xia, H. Jin, Y. Zheng and S.-Z. Qiao, *ACS Catalysis*, 2019, **9**, 2902-2908.
2. J. Wang, D. Wu, M. Li, X. Wei, X. Yang, M. Shao and M. Gu, *Nano Letters*, 2022, **22**, 5600-5606.
3. G. Kresse and J. Furthmüller, *Computational materials science*, 1996, **6**, 15-50.
4. G. Kresse and J. Furthmüller, *Physical review B*, 1996, **54**, 11169.
5. P. E. Blöchl, *Physical review B*, 1994, **50**, 17953.
6. J. P. Perdew, K. Burke and M. Ernzerhof, *Physical review letters*, 1996, **77**, 3865.
7. S. Grimme, J. Antony, S. Ehrlich and H. Krieg, *The Journal of chemical physics*, 2010, **132**, 154104.
8. V. Wang, N. Xu, J.-C. Liu, G. Tang and W.-T. Geng, *Computer Physics Communications*, 2021, **267**, 108033.
9. P. Wei, J. Liang, Q. Liu, L. Xie, X. Tong, Y. Ren, T. Li, Y. Luo, N. Li, B. Tang, A. M. Asiri, M. S. Hamdy, Q. Kong, Z. Wang and X. Sun, *Journal of Colloid and Interface Science*, 2022, **615**, 636-642.
10. R. Zhang, Y. Guo, S. Zhang, D. Chen, Y. Zhao, Z. Huang, L. Ma, P. Li, Q. Yang, G. Liang and C. Zhi, *Advanced Energy Materials*, 2022, **12**, 2103872.
11. H. Du, H. Guo, K. Wang, X. Du, B. A. Beshiwork, S. Sun, Y. Luo, Q. Liu, T. Li and X. Sun, *Angewandte Chemie International Edition*, 2023, **62**, e202215782.
12. Q. Yin, S. Hu, J. Liu and H. Zhou, *Sustainable Energy & Fuels*, 2022, **6**, 4716-4725.
13. X. Yang, R. Wang, S. Wang, C. Song, S. Lu, L. Fang, F. Yin and H. Liu, *Applied Catalysis B: Environmental*, 2023, **325**, 122360.
14. X. He, J. Li, R. Li, D. Zhao, L. Zhang, X. Ji, X. Fan, J. Chen, Y. Wang, Y. Luo, D. Zheng, L. Xie, S. Sun, Z. Cai, Q. Liu, K. Ma and X. Sun, *Inorganic Chemistry*, 2023, **62**, 25-29.